Article:
Fukagai, S., Ma, L. and Lewis, R. (2019) Tribological approach to optimize traction coefficient during running-in period using surface texture. Wear, 424-425. pp. 223-232. ISSN: 0043-1648

https://doi.org/10.1016/j.wear.2019.02.023

TRIBOLOGICAL ASPECTS TO OPTIMIZE TRACTION COEFFICIENT DURING RUNNING-IN PERIOD USING SURFACE TEXTURE

Shinya Fukagai [1, 3*], Le Ma [2], Roger Lewis [1]

[1] Leonardo Centre for Tribology, Department of Mechanical Engineering, University of Sheffield, Sheffield, UK

[2] Sorby Centre, Department of Materials Science and Engineering, University of Sheffield, Sheffield, UK

[3] Railway Technical Research Institute, Tokyo, Japan

Abstract

Risk of wheel-climb derailment increases if the traction coefficient in the wheel/rail contact is too high. This has been observed to happen more just after wheel turning. This novel work investigates how the traction coefficient rises during the running-in period, when textured surfaces are used to simulate a freshly turned wheel. Running-in curve of traction coefficient showed a momentary rise and a peak value of traction coefficient was observed to decrease with the increase in magnitude of the wheel surface texture. The change of the subsurface hardness and the microstructure were also dependent on the initial surface texture coincidentally and the work-hardening layer of the textured surface was thicker than that of smooth surface. A mechanism model of the effects of surface texture on traction characteristics during the running-in was presented. The work will allow recommendations of wheel turning to be made to help reduce the problem of wheel-climb derailment.

Keywords: running-in; traction coefficient; surface texture; plastic deformation; subsurface structure; flange climb.

1. Introduction

Since the frictional condition between railway wheel and rail has an important role in the transmission of driving force and braking force, it should be kept at a high level to secure the appropriate acceleration performance and braking distance. On the other hand, the risk of wheel climb derailment will be increased if the traction coefficient is too high at sharp curves because it generates a greater force in the lateral direction, namely toward to the outside of a curve. The force presses the wheelset against the gauge corner of the outer rail and could cause the flange to climb up [1][2][3]. Therefore, it is important to understand the phenomenon and appropriately control the friction condition. The general method to control the friction condition is the application of lubrication between the wheel and rail. However, installation of lubrication equipment or work by hand at the depot would make an additional expense and a significant contamination around the bogie. Moreover, excessive lubrication causes slips.

A railway wheel experiences re-profiling several times during its whole life to reset it to the designed profile from the worn profile or to remove damage, such as wheel flats and cracks. And it is known that some derailments have occurred relatively soon after the re-profiling of wheels [4][5][6][7]. Just after the re-profiling, there are machining marks which depend on the shape of cutting tool and the feed rate at the wheel surface. Some reports mention the possibility that the rougher surface leads to a higher traction coefficient and it increases the risk of flange climb derailment [6][7][8]. Namely, they indicate that the spike-like machining marks cause an increase of traction during the running-in period as they plough into the rail material. Therefore, a smooth surface is recommended at the finishing of wheel machining sometimes [6][8]. On the other hand, there is another opinion that mentions that the traction force is increased with the deformation of machining marks and increase in real contact area [4], which means that adhesion predominantly affects the increase. Though the mechanism for the traction behaviour during running-in has not been clarified well, there are experimental results using a twin-disk test machine to investigate the influence of the surface texture on the traction characteristics as follows.

Yamamoto *et al.* reported that the traction coefficient of the interface between wheel tread/top of rail could be reduced by optimizing the texture using twin disk tests [9][10]. They indicated that application of these textures to a wheel during turning might reduce the risk of derailment. Therefore, there is a possibility to optimize the surface treatment of wheels by the use of the existing re-profiling equipment with more detailed investigation about the mechanism. Especially, which

---

* Corresponding author
E-mail: fukagai.shinya.81@rtri.or.jp

friction condition between wheel flange/rail gauge corner contact would relate best to the wheel climb derailment. Lundmark *et al.* carried out some case studies of frictional behaviour using different initial roughness and reported that the combination of a rough wheel disk and a smooth rail disk showed the lowest traction coefficient [11]. As a possible reason, the influence of a small difference in the hardness of the work-hardened layer of a rough wheel was indicated. It is well known that the transitions in frictional behaviour during running-in are influenced by not only the change of surface topography. They can also relate to changes in surface composition, microstructure and third-body layer, depending on the environment. Blau also indicated that the crystallographic reorientation and the surface conformity could be possible causes to characterize the running-in behaviour on metal-metal friction [12][13]. Baek *et al.* reported that the work-hardening and tribochemical reactions near the surface affect the transition of the traction coefficient differently between dry and wet conditions [14][15][16]. However, it has not been fully understood. To control the traction characteristics and provide a better solution to the flange climb derailment, understanding the behaviour at the interface of wheel/rail during the running-in period and generalizing the model is important.

The aim of this work was to investigate the effects of applying surface texture on traction characteristics during the running-in period and to analyze the tribological mechanisms causing the effect under dry conditions. The tests were carried out using a twin-disk machine. Conditions that simulated the wheel flange/rail gauge corner contact were used. After the tests, the used disks were investigated using an optical surface measurement system (InfiniteFocusSL, Alicona) and a contact-type roughness meter (Surfcorder SE3500, Kosaka Laboratory Ltd.), a micro-Vickers hardness testing machine (Durascan, Struers), optical microscope (Axio Observer, ZEISS), an FEG-SEM (Inspect F50, FEI) with EBSD (Oxford Instrument) and an XPS surface analysis instrument (Supra, Kratos Analytical). The wear debris generated during the test was also collected and the amount was investigated. Finally, mechanistic modelling was presented to explain the effect of surface texture. These findings might inform rail service providers about optimal wheel profiling methods and surface treatments to reduce the likelihood of wheel climb derailments.

2. Methodology

2.1. Apparatus

Figure 1 shows a schematic diagram of the twin-disk rolling-sliding test machine [9][10][14][15][16], which is equipped with a small wheel disk and rail disk, and Table 1 shows the performance of the experimental apparatus. The wheel disk and the rail disk are connected to separate servomotors. These motors rotate independently and the slip ratio between the disks is prescribed by setting different rotational speeds for each motor. The braking motor is supported by a linear guide that can move in the axial direction. The vertical load is applied to the test disks by use of a coil spring.

[Figure 1 about here.]

[Table 1 about here.]

2.2. Test disks

Figure 2 shows the shape and dimension of the test disks. They were cut from actual railway wheels and rails; SSW-Q3S (JIS E 5402) and 50N (JIS E 1101) for the wheel and rail, respectively. In order to simulate the wheel flange/rail gauge corner contact, the wheel disk was made to be a “conical” shape and the rail disk was made to be a “crowned” shape. The straight section of actual wheel flange is 60 -70 degrees. However, the contact between wheel flange and rail gauge corner will take place at not only the straight section, but also the flange root. Therefore, the angle will change from approximately 0 to 70 degrees. Since this is the first trial to evaluate the traction coefficient in the direction for the derailment, the taper angle of wheel disk was chosen as 45 degrees for manufacturing reasons in this study. The shape was designed to have the same radius, 30 mm, at the contact point. Figure 3 shows the surface profiles of the test disks which were obtained using a contact-type roughness meter. Three different types of wheel disks were prepared through surface finishing operations. Disk-A is the most smooth surface which was acquired by grinding. Since the railway wheel is generally re-profiled by use of a machining tool, the micro texture disks B and C were applied this technique; 0.5 mm/rev and 1.0 mm/rev tools pitch were used for disk-B and disk-C, respectively. The direction of machining was parallel to the direction of disk rotation. This means that the machining marks were oriented across the direction of rotation to simulate the actual machining situation of the wheel. Rail disks had just one type of surface which was acquired by grinding. Table 2 shows the characteristics of disk surfaces. The roughness values were obtained using a roughness meter.

[Figure 2 about here.]

[Figure 3 about here.]

[Table 2 about here.]

2.3. Test procedure

Table 3 shows the experimental conditions. In general, the Hertzian maximum contact pressure at the wheel flange/ rail gauge corner is up to 2700 MPa [17]. Accordingly, the standard contact pressure was set at 2200 MPa. The standard speed was set at 0.16 m/s; this was done to avoid resonance in the experimental apparatus. From the considerations of the contact situation at the wheel flange/rail gauge corner, the standard slip ratio and angle of attack were set at 2% and 1°, respectively. These values were defined by the results of preliminary simulations of a derailment.

[Table 3 about here.]

The surfaces of the test disks were washed with petroleum ether in an ultrasonic washing vessel before the experiments to remove contaminants such as oil and dust. Figure 4 shows a set of wheel and rail disks after attachment on the experimental apparatus. In the experimental apparatus vertical load V and lateral load L were measured; but for detecting the traction coefficient in the lateral direction, these were used to determine the normal force N and the lateral traction force in the lateral direction F_y with the following equations:

$$N = V\cos\alpha + L\sin\alpha, \quad (1)$$

$$F_y = V\sin\alpha - L\cos\alpha \quad (2)$$

where α is the contact angle (45° in this experiment).

[Figure 4 about here.]

The surface profile was measured at different stages, the detail of stage is to be mentioned in next section, using an optical surface measurement system that had a vertical resolution of 50 nm and a contact-type roughness meter that had a vertical resolution of 200 nm. For the quantification of the plastic deformation by means of hardness, HV0.05 hardness profiles were performed from the deformed near-surface zone into the bulk using a micro-Vickers hardness testing machine. The metallic structures of cross sections were observed by an optical microscope and FEG-SEM with EBSD. Acceleration voltage of SEM and EBSD was 20 keV and spot size was 5 μm. The chemical component on the surface was analyzed by an XPS surface analysis instrument with a monochromated aluminium source. An Ar_{500}^{+} at 20 keV source was used to etch away the surface for 300 seconds, and then restricted high resolution scans were collected over the O 1s and Fe $2p_{3/2}$ regions. This was repeated 10 times to build up a depth profile. The Ar_{500}^{+} source at 20 keV has been shown to have an etch rate of 8.3 nm/min through Ta_2O_5 on Ta. During the experiments, a tray was left under the specimens and the amount of wear particles was evaluated.

3. Results

3.1. Effect of initial surface texture on traction coefficient

Figure 5 shows the change of traction coefficient in the lateral direction with running time. The tests were carried out three or four times at the same condition and it was shown that there was the reproducibility for every type of wheel disk. It was found that the change of traction coefficient depends on the initial surface texture. Though every type of wheel disk showed a momentary rise in traction coefficient during running-in, the rougher the initial surface profile was, the smaller the peak value of traction coefficient was. Figure 6 shows the schematic patterns of the traction coefficient curve in Fig. 5. “Stage-I” means the condition before the test, “stage-II” means the condition around the peak of the traction coefficient and “stage-III” means the condition after the test. The rougher the initial surface profile was, the longer time took it to reach the peak value. Hereinafter, the analysis of the disks for each characteristic stage (I, II and III) were carried out. Here, the analysis for stage-II was carried out by discontinuing a test after confirming the reproducibility of the change of traction coefficient.

[Figure 5 about here.]

[Figure 6 about here.]

3.2. Surface texture

Figure 7 shows the change of surface topography of wheel disk and rail disk for each stage which was obtained using an optical surface measurement system. It is clearly shown that the surface deformation increased with the progress of stage and the direction of plastic flow corresponded to that of traction force in the lateral direction for every type of wheel disks. The initial ridges of disk-B and disk-C were almost made flat at stage-II. Though disk-B and -C seems to proceed the conformity with the progress of stage, the surface of disk-A at stage-III seems to be rougher than that at stage-II.

[Figure 7 about here.]

Figure 8 shows the surface profile of test disks for each initial surface profile and stage which was obtained using the contact-type roughness meter. It was found that the surface shapes of the wheel disk and the rail disk went close to the similar shapes each other by the generation of traction force in the lateral direction. It appeared this conformation of the surface profile progressed with the progress of stages and the shape at the stage-III was similar in all initial surface profiles.

Disk-C showed that more or less only one spike was in contact. The radius of the actual rail gauge corner is 13 mm, and the machining pitch of an actual wheel is about 1 – 2 mm. The radius of this rail specimen was 10 mm, and the machining pitches of the wheel specimen were 0.5 and 1 mm. Therefore, the geometry of cross-section is reasonable. One of authors reported that the actual contact shape was made of a few strips by tests using a full-scale wheel/rail contact machine and the result of this study agrees with that [18].

[Figure 8 about here.]

3.3. Hardness

Figure 9 shows the depth profile of hardness of test disks for each initial surface profile and stage. Comparing depth profiles of all disks at stage-II, it was found that the largest increase of hardness near the surface was on disk-C followed in order by disk-B and disk-A. The cause of the increase for the disk-C and disk-B seems to be the larger plastic deformation of the ridges which will be followed by work-hardening than disk-A, because the higher the ridges are more easily deformed.

[Figure 9 about here.]

3.4. Metallic structure

Figure 10 shows the metallic structures observed by optical microscope for each initial surface profile and stage. It is clearly shown that the plastic deformation was increased with the progress of stages for all disks. At stage-II, the depths of plastic flow (white arrows) of disk-B and disk-C were approximately 70 μm. On the other hand, that of disk-A would not be clearly seen beneath the surface. There was no difference among the disks at the point of stage-III, the depth of plastic flow of disk-B and disk-C were approximately 100 μm and that of disk-A was 90 μm. These appearances correspond to the results of the depth profile of hardness.

[Figure 10 about here.]

Figure 11 shows the sub-surface EBSD plots for wheel disk-A and disk-C at stage-II; (i) shows the inverse pole figure (IPF) for a visualisation of the structure of lattice domains (grains) with grain boundaries (low-angle (>5°) grain boundaries LAGB area thin black line and high-angle (>15°) grain boundaries HAGB area bold black line); (ii) shows the combined plot of pattern quality and grain boundaries (low-angle (>5°) grain boundaries LAGB area thin red line and high-angle (>15°) grain boundaries HAGB area bold black line); (iii) shows the local misorientation for the intergranular deformation (rainbow-scale from 0° to 5°).

[Figure 11 about here.]

It was clearly found that both generated plastic flow in the direction of the traction force, even in disk-A which was not confirmed in Fig. 10. Figure 11 (i) and (ii) show that the closer to the surface, the smaller the grain size was and Fig. 11 (iii) shows that the closer to the surface, the more significant the strain that was generated for both disks. It appeared that the closer to the top surface, the more the data are missing, it means that the increase of dislocation density and significant decrease of grain size occurred by the large shear stress. These results visualize the formation of pronounced plastic flow. The thickness of the layer which was affected by plastic flow of the disk-C was approximately 70 μm and that of disk-A was more significant thinner, at approximately 15 μm.

3.5. Amount of wear particle

Figure 12 shows the amount of wear particles during experiment which was captured under the disks. These results show that there was almost no generation of wear particles between stage-I and stage-II and a large amount was generated between stage-II and stage-III. It would indicate that the surface roughness was deformed plastically until completing the

conformation of surfaces and the adhesive wear started after that. There is almost no difference in the amount of wear particles throughout the experiments, from disk-A to disk-C.

[Figure 12 about here.]

3.6. Chemical composition

Figure 13 shows the depth profile of the oxygen concentration to iron concentration for each initial surface profile and stage which was obtained using XPS. The depth profiles were collected from the same area. Though there was a slight difference of the oxygen concentration profile for each initial surface profile at stage-I, it is possible that a scattering of initial surface conditions caused the difference. On the other hand, there was no difference at stage-II and -III. It indicates that the oxidation state became similar soon after starting the test and progressed in the almost same way during each test. There is a tendency for the oxidation to increase with the progress of the test in all disks.

[Figure 13 about here.]

Figure 14 shows the high-resolution Fe 2p spectrum for the wear track on samples for stage-III. The iron oxide can be distinguished by the peak positions within the Fe 2p high resolution spectra, and also by the presence and position of additional satellite peaks [19] which are generated by the excitation of outer-shell electrons following the excitation of the core electron. Fe_3O_4 is not expected to show a satellite feature whilst Fe_2O_3 is expected to show a significant feature at 719 eV. Regarding the Fe $2p_{3/2}$ XPS peak positions, this peak is expected at 711.0 eV for Fe_2O_3, 710.6 eV for Fe_3O_4 and approximately 709.0 eV for FeO. Fe metal is expected at approximately 706.7 eV. The Fe 2p spectra shown here for the wear tracks appear to show little or no satellite features, suggesting the oxide is predominantly Fe_3O_4 and this is consistent with the Fe $2p_{3/2}$ peak position at approximately 710.6 eV for these samples.

[Figure 14 about here.]

4. Discussion

The results of the twin-disk tests which simulated the wheel flange/rail gauge corner contact showed that the machining pitch of the wheel strongly influences the traction characteristics during the running-in period. The larger the machining pitch was, the smaller peak value of traction coefficient was. As mentioned in Chapter 1, it is sometimes believed that the spike-like machining marks cause an increase of traction during the running-in period. However, the results of this work contradict this and show that rougher wheel surfaces give lower traction coefficients.

Doi *et al.* [4] mentioned the possibility, that the traction coefficient could rise when the machining pattern was worn out from the results of field tests, and it agrees with the results of these laboratory tests. On the other hand, Kataori *et al.* [5] mentioned that the influence on the rise of the traction coefficient by the different machining pitch did not appear in the field tests. However, it might be hidden by the dispersion of the test conditions, such as the presence of dust, humidity, temperature and surface condition of actual wheel and rail because making steady test conditions at field sites is quite difficult. Since the test conditions for these laboratory tests were well controlled, it is thought that the influence was elicited.

As the results of microstructural analysis for the surface showed, the evolution of plastic flow was found on every type of specimen around near-surface region with the progress of the stages. At stage-II, the samples which had a longer machining pitch showed a deeper range of plastic flow beneath the contact point. Corresponding to this evolution of plastic flow, the depth profile of the hardness indicated that the long pitch surface generated more significant work-hardening than the grinned surface. Figure 15 shows a schematic model of the effects of surface texture on traction characteristics during the running-in period.

[Figure 15 about here.]

From stage-I to stage-II, the surface asperities were deformed plastically and the resistance to deformation was dependant on the traction force. The fact that the amount of wear particles was extremely small between stage-I and stage-II indicates that the surface was under going shake-down. It is also known that the presence of significant flow in the bulk gives a saturation of coefficient of friction with the increase of contact pressure [20][21][22]. Here, disk-B and disk-C, which had a machined surface, produced higher contact pressure than disk-A because of their conformational factor and suppressed the increase in traction coefficient. Comparing metallic structures of all kinds of disks at stage II, it was found that disk-A had a quite small magnitude of plastic flow compared with disk-B and disk-C. It is thought that disk-B and disk-C were more easily plastically deformed and shake-down settled down earlier than disk-A.

From stage-II to stage-III, the traction coefficient decreased in the case of disk-A, and slightly decreased and maintained in the case of disk-B and disk-C. In order to discuss the phenomenon, the Bowden-Tabor model on boundary friction [23] was applied as same as used by Halling [24] and Baek *et al.* [14]. Since the cycle of shake-down changed the interfacial condition from a plastic contact to an elastic contact, the traction coefficient can be expressed by the following formula with the concept of adhesion [14]:

$$\mu = \frac{\tau_c}{H_{eff}} \tag{3}$$

where, τ_c is the shear strength of the contact interface and H_{eff} is the effective hardness. The effective hardness is the hardness involving the surface layer and it is different from the hardness of either the layer or substrate material. The effective hardness depends on the thickness of the surface layer and it closes to the layer hardness with the increase of thickness. In the case of disk-C (and B), (i) the plastic deformation near the surface dramatically evolves and the thick plastic flow layer is quickly formed between stage-I and stage-II, (ii) traction coefficient make a settlement with the high τ_c and H_{eff} between stage-II and stage-III. On the other hand, in the case of disk-A, (i) plastic deformation relatively slowly progresses and the thin plastic flow layer is formed between stage-I and stage-II, (ii) traction coefficient shows high value because of high τ_c and low H_{eff} and it decreases with an additional evolution of plastic deformation, which increases H_{eff}, between stage-II and stage-III.

As shown in Fig. 11, the extreme surface for both (a) Disk-A and (b) Disk-C showed significant deformation at stage-II, and similar dislocation density which is represented in grain size, grain boundaries and local misorientation. On the other hand, there was a significant difference in the depth of plastic flow. The depth of plastic flow of Disk-C, 70 μm, was approximately five times larger than that of Disk-A, 15 μm. It means that the difference of effective hardness H_{eff} is larger than that of shear strength τ_c between disk-A and disk-C.

Moreover, the generation of a third-body layer, which consisted of oxides such as magnetite, was another factor to make a reduction in traction coefficient for all disks. It has been reported that the existence of third body layer would influence the traction characteristic [25] and especially magnetite could work as a self-lubricated film and prevent the increase in traction coefficient [16][26].

5. Conclusions

Investigations of a twin-disk test machine revealed a tribological phenomenon between textured wheel and rail materials during running-in period. The results of experiments and analysis are summarized as follows:

1. The twin-disk tests, which simulated the wheel flange/rail gauge corner contact, showed that the machining pitch of the wheel strongly influences the traction characteristics during the running-in period. The larger the machining pitch was, the smaller peak value of traction coefficient was. It is sometimes believed that the spike-like machining marks cause an increase of traction during the running-in period. However, the results of this work contradict this and show that rougher wheel surfaces give lower traction coefficients.
2. The microstructural analysis around the near-surface region of the characteristic stages, such as before test (stage-I), around the peak point of traction coefficient (stage-II), after test (stage-III), showed evolution of plastic flow was found on every type of specimen with the progress of stages.
3. At stage-II, the samples which had a longer machining pitch showed a deeper range of plastic flow beneath the contact point. Corresponding to this evolution of plastic flow, the depth profile of hardness indicated that the long pitch surface generated more significant work-hardening than the unmachined surface.

Based on the above results, a mechanism model of the effects of surface texture on traction characteristics during running-in period was proposed. It is considered that the major factors causing a decrease in the transient traction coefficient are plastic deformation of the surface texture. And the difference of peak value was generated by the difference of the depth of plastic flow. Above results indicate that there might be an appropriate texture or surface treatment to reduce the risk of flange climb derailment during running-in.

References

[1] W.C. Shust, J.A. Elkins, Wheel forces during flange climb part I - track loading vehicle tests, in: Railr. Conf. 1997., Proc. 1997 IEEE/ASME Joint., 1997: pp. 137–147.

[2] H. Ishida, T. Miyamoto, E. Maebashi, H. Doi, K. Iida, A. Furukawa, Safety Assessment for Flange Climb Derailment of Trains Running at Low Speeds on Sharp Curves, Q. Rep. RTRI. 47 (2006) 65–71. doi:10.2219/rtriqr.47.65.

[3] A. Matsumoto, Y. Sato, H. Ohno, M. Tomeoka, K. Matsumoto, T. Ogino, M. Tanimoto, Y. Oka, M. Okano, Improvement of bogie curving performance by using friction modifier to rail/wheel interface Verification by full-scale rolling stand test, Wear. 258 (2005) 1201–1208. doi:10.1016/j.wear.2004.03.063.

[4] H. Doi, T. Miyamoto, J. Suzumura, J. Nakahashi, H. Chen, T. Ban, Change in Surface Condition of Turned Wheel and Effectiveness of Lubrication Turned against Flange Climb Derailment, Q. Rep. RTRI. 53 (2012) 70–76.

[5] A. Kataori, K. Doi, H. Iijima, S. Momosaki, S. Matsumoto, The Influence of the Wheel/Rail Contact Point Condition on Friction Coefficient, 9th World Conf. Railw. Res. (2011).

[6] S. Greene, G. Cook, N.P. Ford, R.L. Freeland, F.M. Gilliam, J. a Hough, R.H. Irwin, G.G. Bridge, D. a Lee, Flange Climb Derailment criteria and Wheel/Rail Profile management and Maintenance Guidelines for Transit Operations, 2005.

[7] S. Iwnicki, Handbook of railway vehicle dynamics., CRC press, 2006.

[8] J. Stow, P. Allen, A Good Practice Guide for Managing the Wheel-Rail Interface of Light Rail and Tramway Systems, Off. Rail Regul. (2008).

[9] D. Yamamoto, H. Chen, A Fundamental Study on Fine Unevenness and Tangent Force on Wheel Tread of Railway Vehicle (Relations between Environmental Condition and Tangent Force Characteristics with a Two-Disk Rolling Machine), Trans. JAPAN Soc. Mech. Eng. Ser. C. 77 (2011) 3211–3222. doi:10.1299/kikaic.77.3211.

[10] D. Yamamoto, H. Chen, Influence of the fine unevenness of wheel tread on the running stability of railway vehicle, Trans. JAPAN Soc. Mech. Eng. Ser. C. 79 (2013). doi:10.1299/kikaic.79.2338.

[11] J. Lundmark, E. Kassfeldt, J. Hardell, B. Prakash, The influence of initial surface topography on tribological performance of the wheel/rail interface during rolling/sliding conditions, Proc. Inst. Mech. Eng. Part F J. Rail Rapid Transit. 223 (2009) 181–187. doi:10.1243/09544097JRRT223.

[12] P.J. Blau, On the nature of running-in, Tribol. Int. 38 (2005) 1007–1012. doi:10.1016/J.TRIBOINT.2005.07.020.

[13] P.J. Blau, Friction and wear transitions of materials, Noyes publications, 1989.

[14] K.S. Baek, K. Kyogoku, T. Nakahara, An experimental study of transient traction characteristics between rail and wheel under low slip and low speed conditions, Wear. 265 (2008) 1417–1424. doi:10.1016/j.wear.2008.02.044.

[15] K.S. Baek, K. Kyogoku, T. Nakahara, An experimental investigation of transient traction characteristics in rolling-sliding wheel/rail contacts under dry-wet conditions, Wear. 263 (2007) 169–179. doi:10.1016/j.wear.2007.01.067.

[16] T. Nakahara, K.S. Baek, H. Chen, M. Ishida, Relationship between surface oxide layer and transient traction characteristics for two steel rollers under unlubricated and water lubricated conditions, Wear. 271 (2011) 25–31. doi:10.1016/j.wear.2010.10.030.

[17] R. Lewis, U. Olofsson, Wheel-rail interface handbook, Elsevier, 2009.

[18] S. Fukagai, T. Ban, K. Makino, M. Kuzuta, Y. Kubota, H. Chen, Measurement of contact area between wheel flange and rail gauge corner using ultrasonic technique, 9th Int. Conf. Contact Mech. Wear Rail/Wheel Syst. (2012) 92–97.

[19] T. Yamashita, P. Hayes, Analysis of XPS spectra of Fe2+ and Fe3+ ions in oxide materials, Appl. Surf. Sci. 254 (2008) 2441–2449. doi:10.1016/j.apsusc.2007.09.063.

[20] M.C. Shaw, A. Ber, P.A. Mamin, Friction Characteristics of Sliding Surfaces Undergoing Subsurface Plastic Flow, J. Basic Eng. 82 (1960) 342–345. doi:10.1115/1.3662595.

[21] T. Wanheim, N. Bay, A.S. Petersen, A theoretically determined model for friction in metal working processes, Wear. 28 (1974) 251–258. doi:10.1016/0043-1648(74)90165-3.

[22] T. Nellemann, N. Bay, T. Wanheim, Real area of contact and friction stress at high pressure sliding contact, 43 (1977) 45–53.

[23] D. Tabor, Junction growth in metallic friction the role of combined stresses and surface contamination, Proc. R. Soc. London. Ser. A. 251 (1959) 378–393. http://rspb.royalsocietypublishing.org/content/royprsb/246/1315/19.full.pdf.

[24] J. Halling, Surface coatings materials conservation and optimum tribological performance, Tribol. Int. 12 (1979) 203–208. doi:10.1016/0301-679X(79)90189-0.

[25] A. Meierhofer, C. Hardwick, R. Lewis, K. Six, P. Dietmaier, Third body layer-experimental results and a model describing its influence on the traction coefficient, Wear. 314 (2014) 148–154. doi:10.1016/j.wear.2013.11.040.

[26] S.R. Pearson, P.H. Shipway, J.O. Abere, R.A.A. Hewitt, The effect of temperature on wear and friction of a high strength steel in fretting, Wear. 303 (2013) 622–631. doi:10.1016/j.wear.2013.03.048.

List of Figures

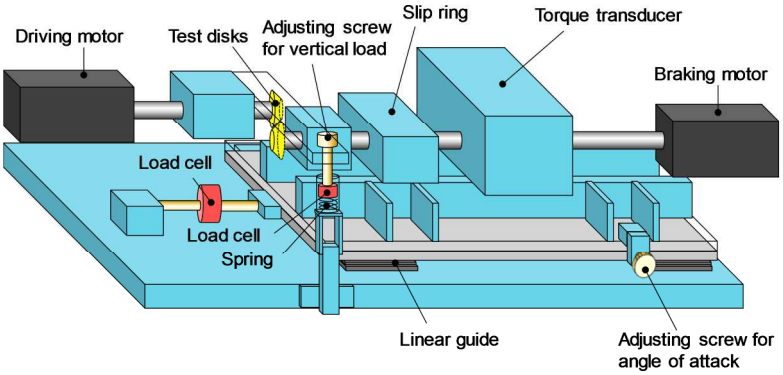

Fig. 1 Schematic diagram of the twin-disk rolling-sliding test machine.

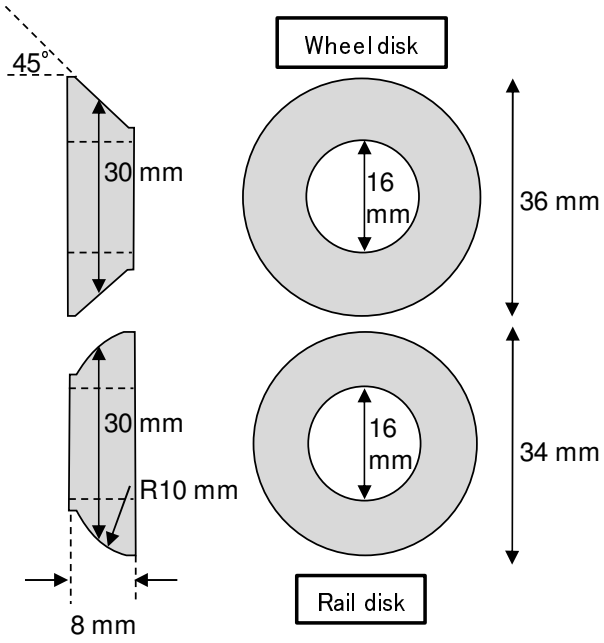

Fig. 1 Shape and dimension of test disks.

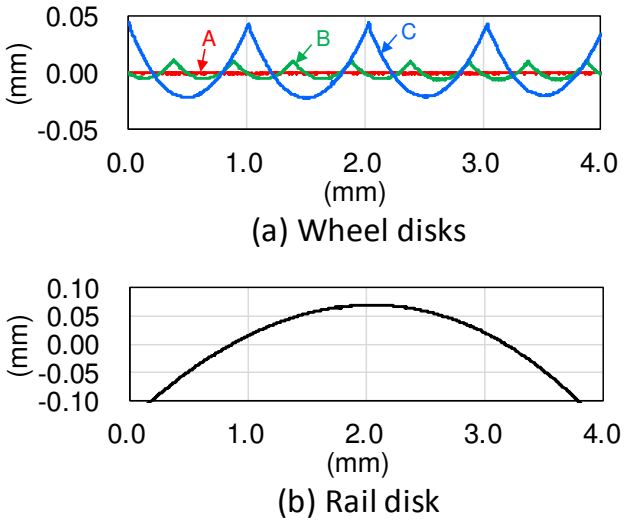

Fig. 3 Surface profile of test disks.

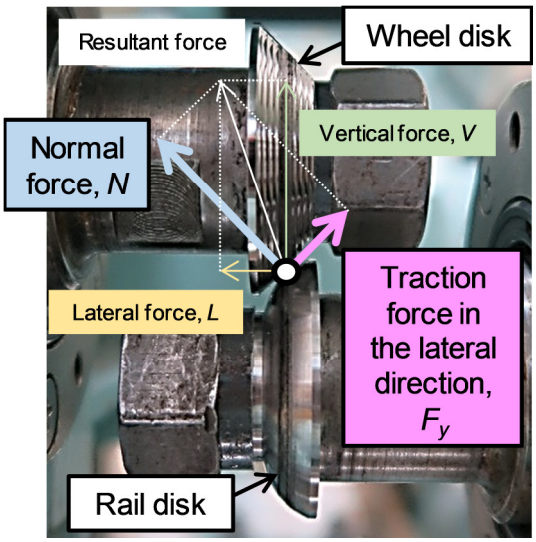

Fig. 4 A set of wheel disk and rail disk after attaching on the experimental apparatus.

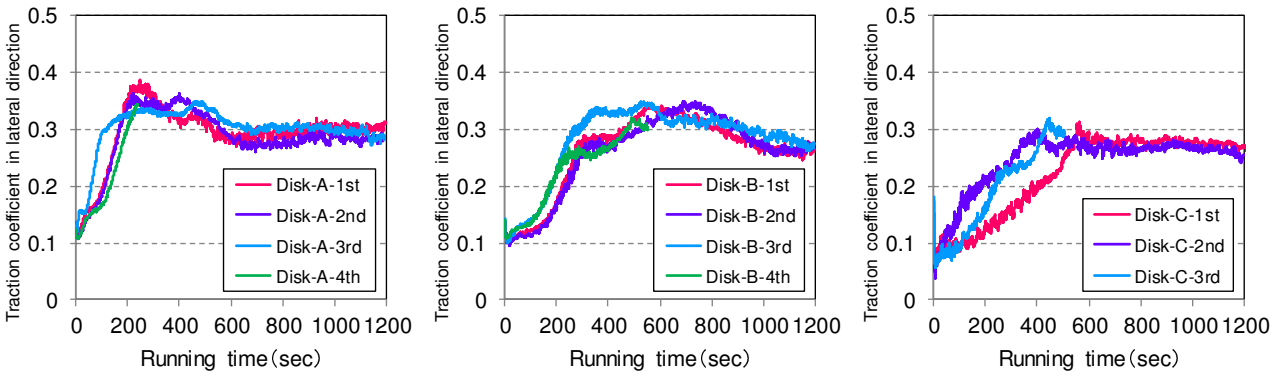

(a) Disk-A (b) Disk-B (c) Disk-C

Fig. 5 Change of traction coefficient in the lateral direction with running time.

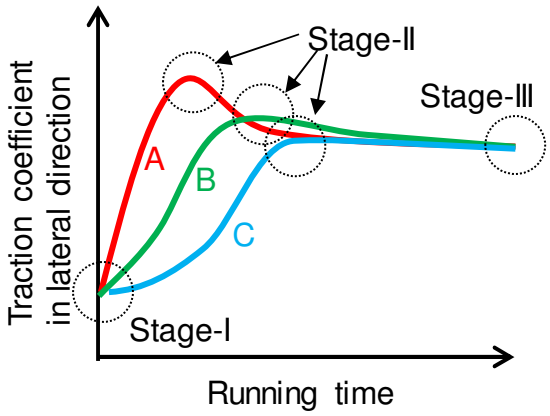

Fig. 6 Schematic patterns of the traction coefficient curves in Fig. 5.

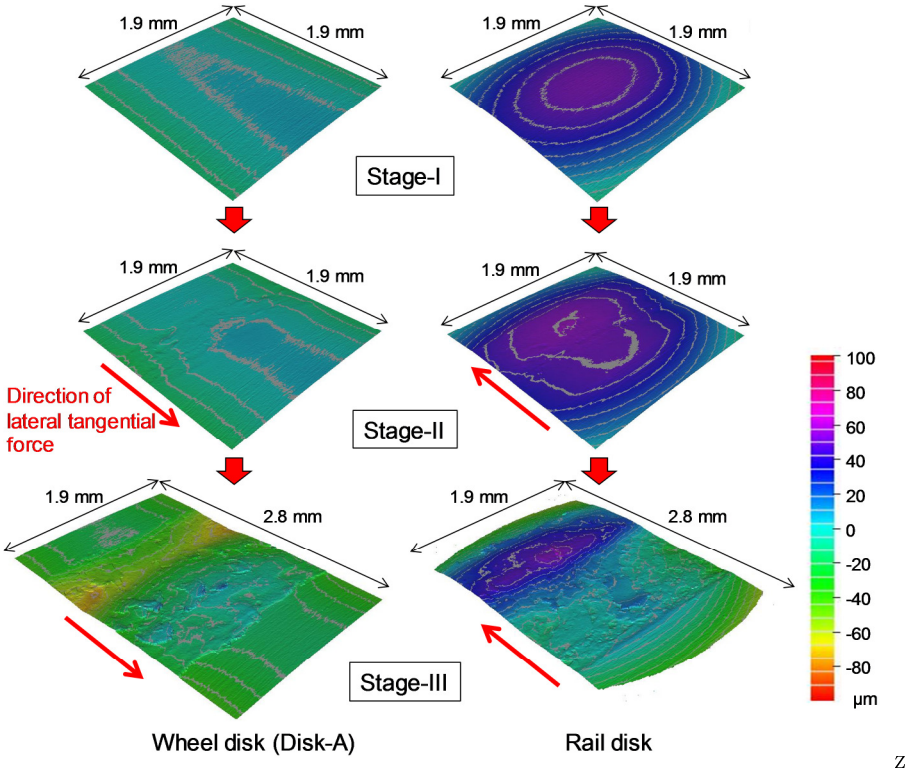

(a) Wheel disk-A and rail disk

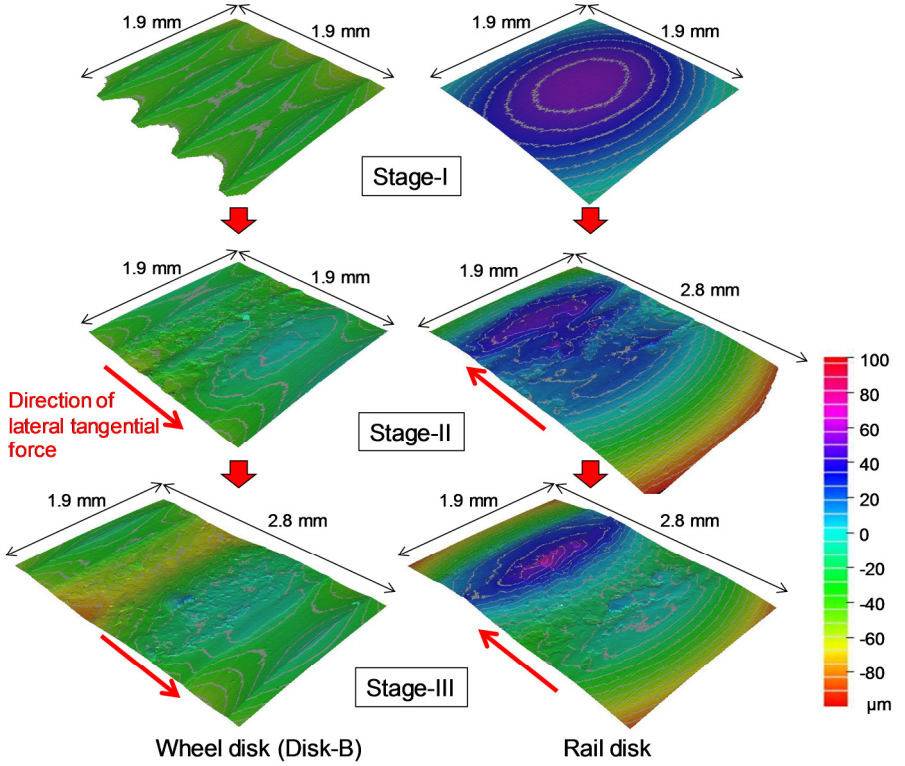

(b) Wheel disk-B and rail disk

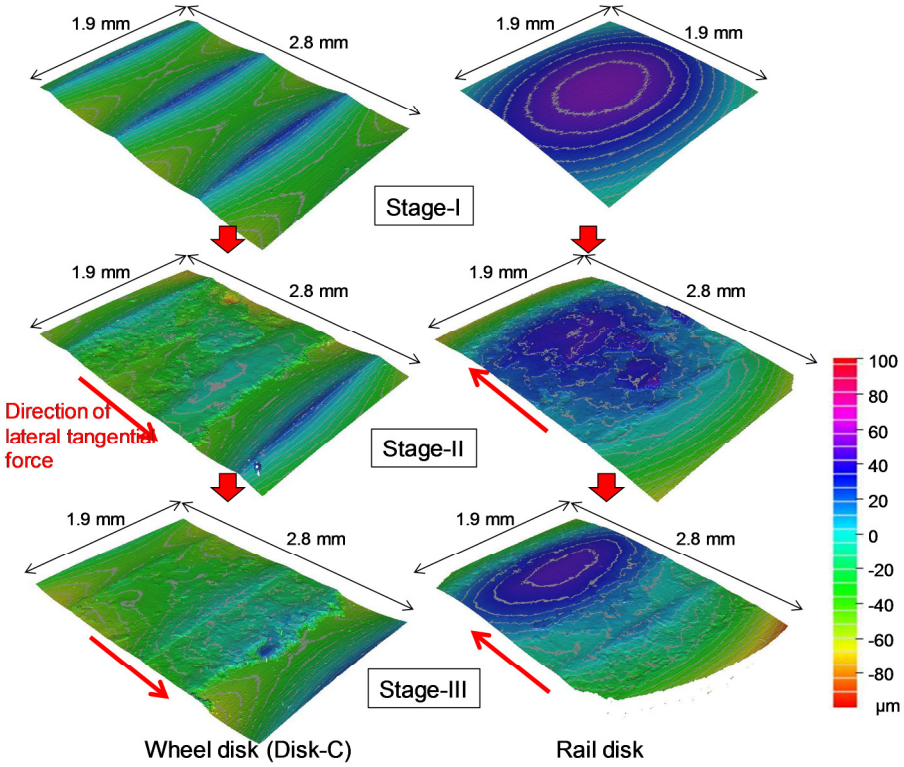

(c) Wheel disk-C and rail disk

Fig. 7 Change of surface topography of wheel disk and rail disk for each stage.

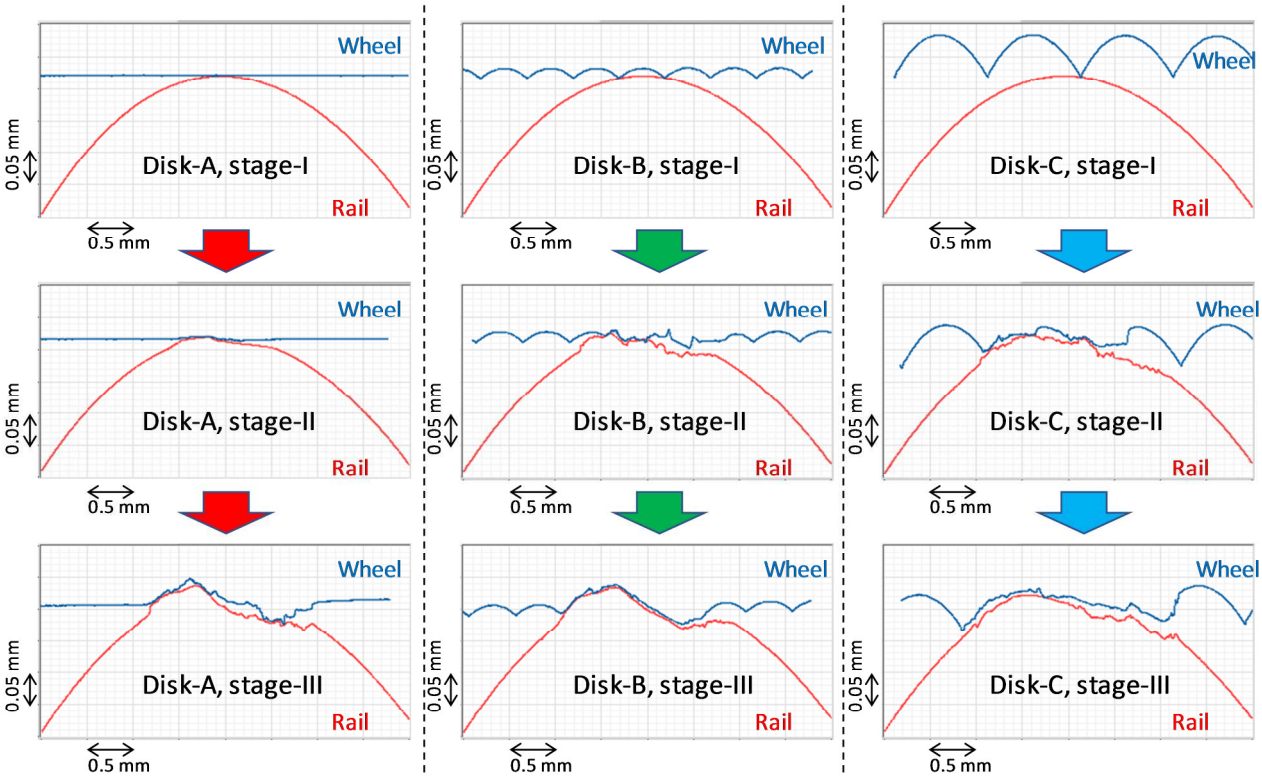

Fig. 8 Surface profile of test disks for each initial surface profile and stage.

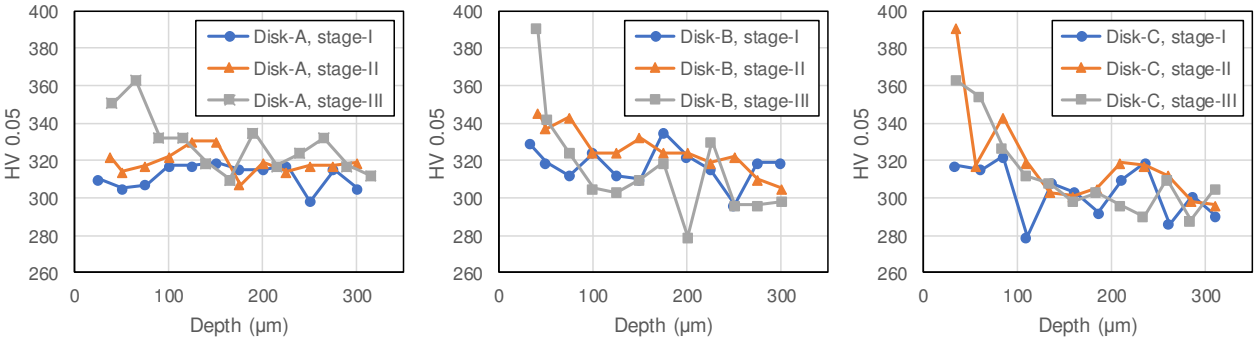

(a) Disk-A (b) Disk-B (c) Disk-C

Fig. 9 Depth profile of hardness of test disks for each initial surface profile and stage.

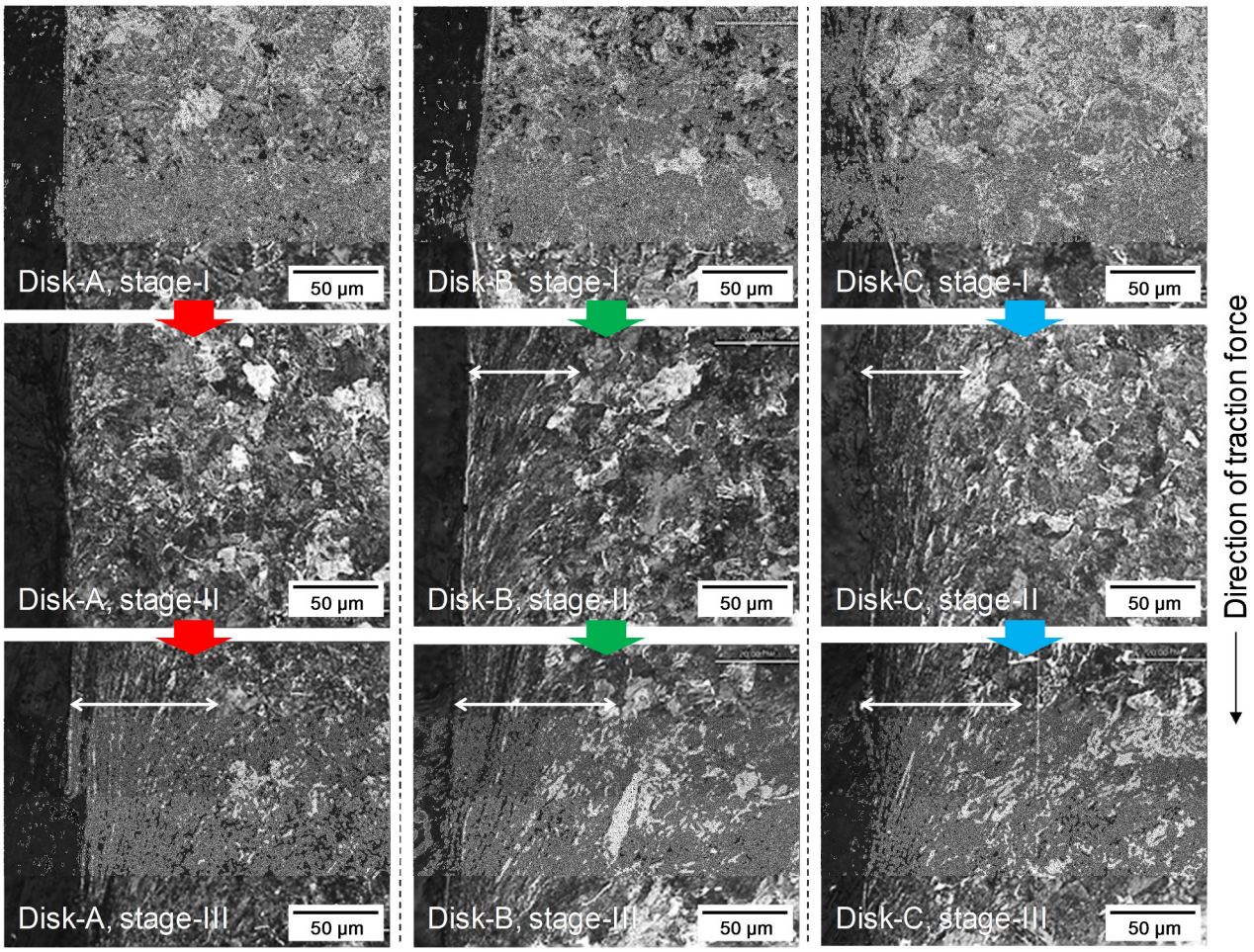

Fig. 10 Metallic structures measured by optical microscope for each initial surface profile and stage.

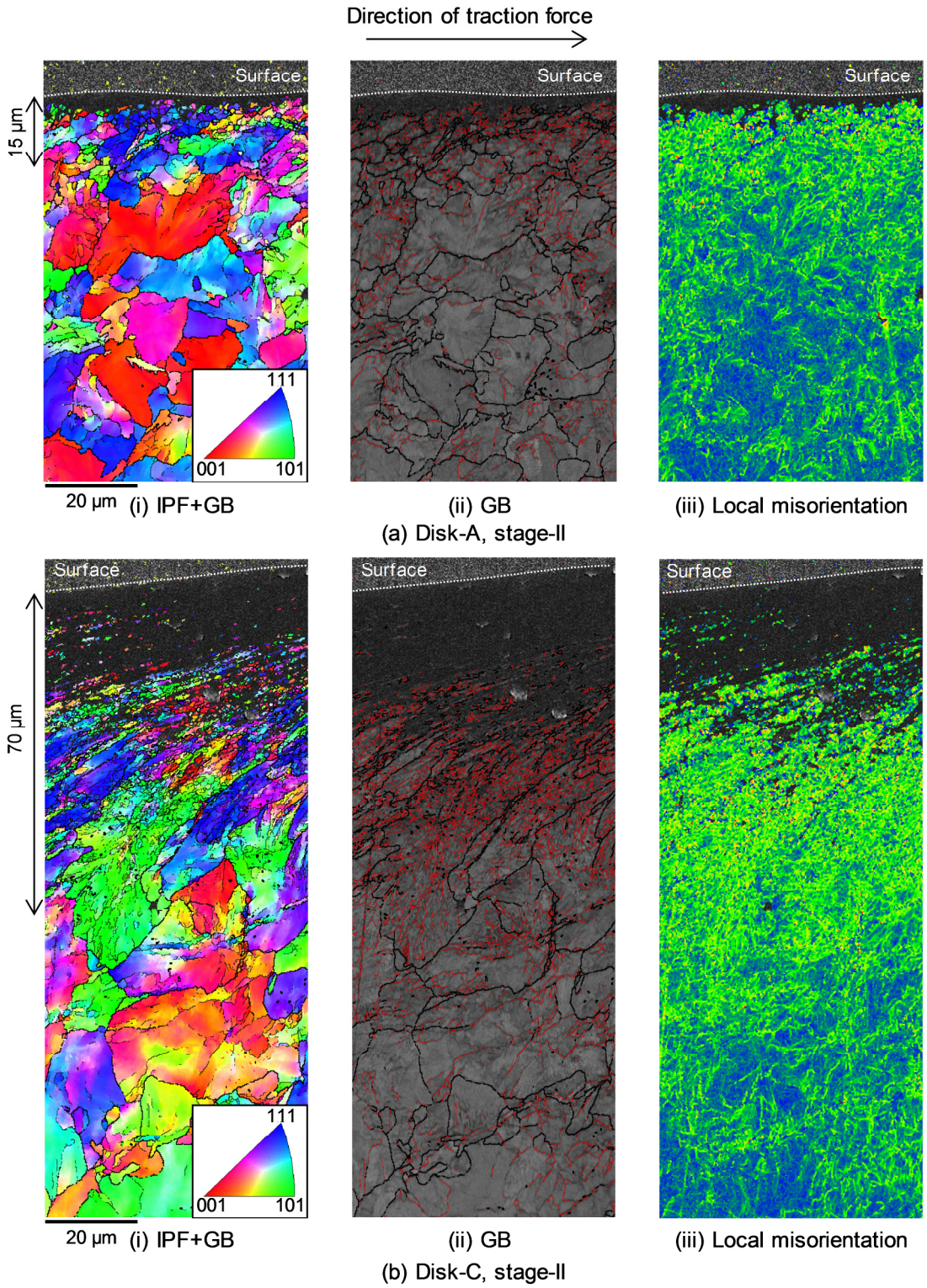

Fig. 11 Sub-surface EBSD plots for wheel disk-A and disk-C at stage-II.

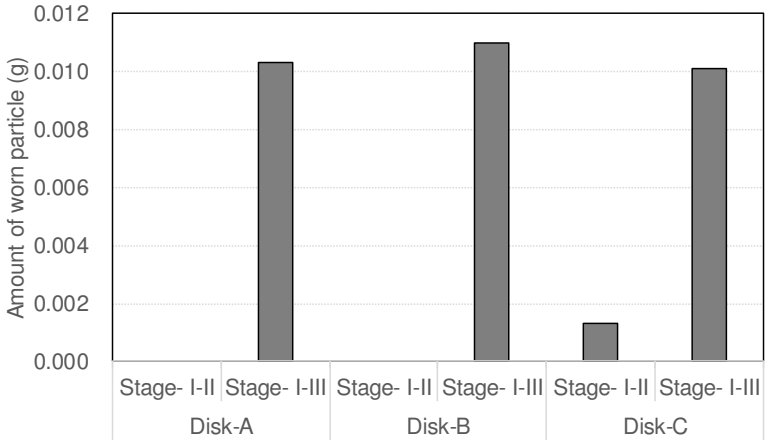

Fig. 12 Amount of wear particle during experiment which was caught under the disks.

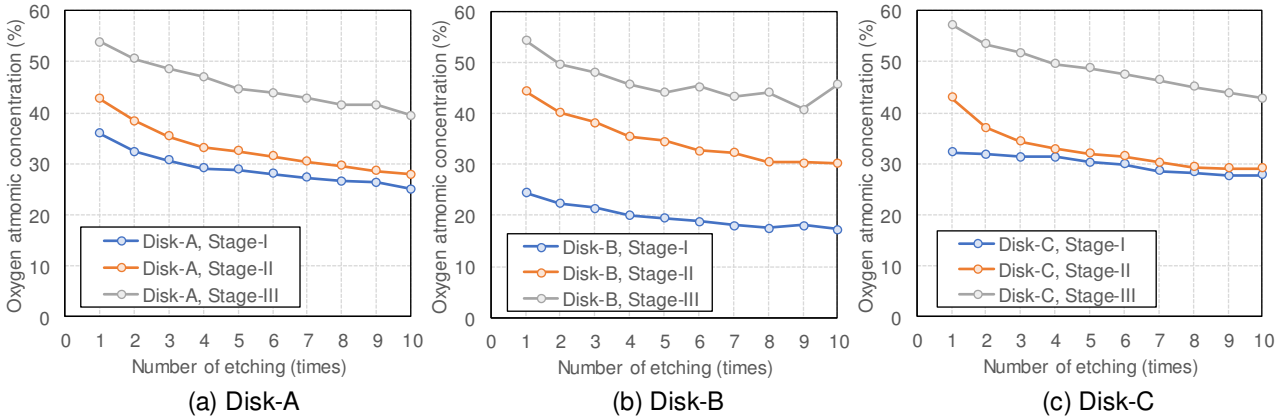

(a) Disk-A (b) Disk-B (c) Disk-C

Fig. 13 Depth profile of the oxygen concentration to iron concentration for each initial surface profile and stage.

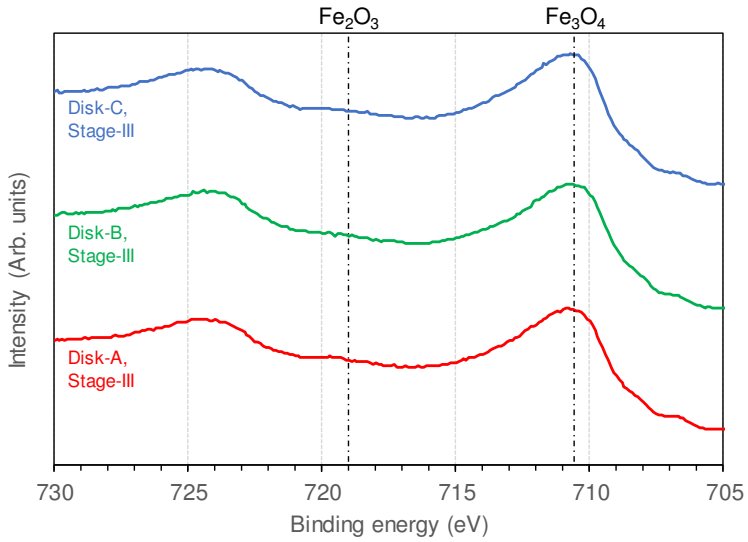

Figure 14 High-resolution Fe 2p spectrum for the wear track on samples of stage III.

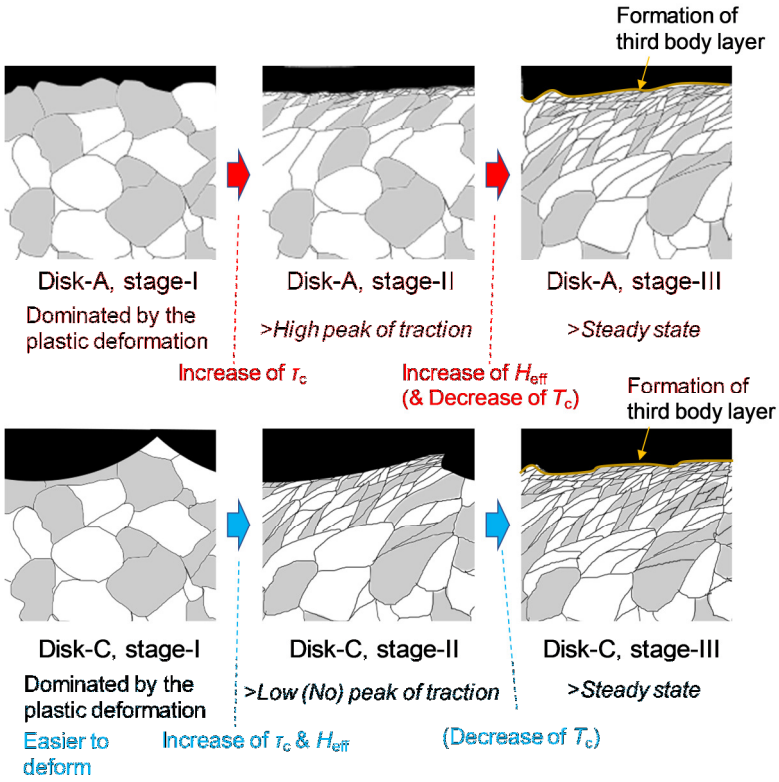

Figure 15 Schematic model of the effects of surface texture on traction characteristics during the running-in period.

List of Tables

Table 1 Performance of the experimental apparatus

Rotational speed (rpm)	0~4000
Vertical load (kN)	0~0.5
Slip ratio (%)	0~5
Angle of attack (°)	-3 to +3

Table 2 Characteristics of disk surface

	Pitch of machining (mm)	Ra (μm)	Pz (μm)
Wheel disk-A	-	0.2	2.2
Wheel disk-B	0.5	3.5	16.7
Wheel disk-C	1.0	6.2	67.1
Rail disk	-	1.1	-

Table 3 Experimental conditions

Rotational speed (rpm / m/s)	100 / 0.16
Vertical load (kN) / Hertzian maximum contact pressure (MPa)	0.3 / 2200
Slip ratio (%)	2
Angle of attack (°)	+1
Room temperature (□)	14.3 - 21.1
Room humidity (RH%)	30 - 34